Colloids, polymers, and needles: Demixing phase behavior

Matthias Schmidt* and Alan R. Denton

Department of Physics, North Dakota State University, Fargo, North Dakota 58105-5566
(Received 3 October 2001; published 23 January 2002)

We consider a ternary mixture of hard colloidal spheres, ideal polymer spheres, and rigid vanishingly thin needles, which model stretched polymers or colloidal rods. For this model, we develop a geometry-based density functional theory, apply it to bulk fluid phases, and predict demixing phase behavior. In the case of no polymer-needle interactions, two-phase coexistence between colloid-rich and colloid-poor phases is found. For hard needle-polymer interactions, we predict rich phase diagrams, exhibiting three-phase coexistence, and reentrant demixing behavior.

I. INTRODUCTION

The richness of phase behavior of systems with purely repulsive interactions depends crucially on the number of components. For a one-component system like colloidal hard spheres, there occurs a freezing transition from a single fluid phase to a dense crystal. Adding a second component, such as nonadsorbing globular polymer coils [1] or rodlike particles [2,3] generates an effective depletion-induced attraction between colloidal spheres, leading to the possibility of demixing. This transition is an analog of the vapor-liquid transition in simple fluids: The phase that is concentrated in one of the components corresponds to a liquid, while the dilute phase corresponds to a vapor, and one frequently refers to such phases as colloidal liquid and colloidal vapor, although the ''vapor'' is concentrated in the added component.

Generic theoretical models for such systems are those introduced by Asakura and Oosawa (AO) and independently by Vrij [1,4], Bolhuis and Frenkel (BF) [5], and Widom and Rowlinson (WR) [6]. The AO model comprises hard colloidal spheres mixed with polymer spheres that are ideal amongst themselves but cannot penetrate the colloids. The BF model adds stiff vanishingly thin needles to a hard sphere system. Because of their vanishing thickness, the needles do not interact with one another. Clearly, both models are similar in spirit, as a noninteracting component is added to hard spheres. In the WR model this is different; two species of spheres interact symmetrically, such that hard core repulsion occurs only between particles of unlike species. Hence a pure system of either component is an ideal gas. All of these model binary mixtures exhibit liquid-vapor phase separation, well established by computer simulations and theories [7–12]. The WR model [6,13–15] has been studied with a range of approaches, including mean-field theory (MFT) [15], Percus-Yevick (PY) integral equation theory [14,16,17], scaled-particle theory (SPT) [18], as well as computer simulations [16,19,20]. The precise location of the liquid-vapor critical point was located by simulations about

50% higher than previously thought [16,19], still a challenge for theories (for a recent integral-equation closure, see Ref. [17]).

In the AO and BF cases a reservoir description has proven to be useful. The reservoir density of either polymers or needles rules the strength of effective attraction and hence plays a role similar to (inverse) temperature in simple substances. Although the WR model features an intrinsic symmetry that seems to preclude such a description, an effective model can also be formulated [15]. In the present paper we consider the phase behavior of a mixture of spheres, polymers, and needles, a natural combination of the above binary cases. We note that our ternary model may provide insight into certain real systems, such as paints, which contain colloidal latex and pigment particles, polymer thickeners and dispersants, as well as many other components [21].

Density functional theory (DFT) [22] is a powerful approach to equilibrium statistical systems, possibly under influence of an external potential. Building on Rosenfield's work [23], a geometry-based approach was recently proposed that also predicts bulk properties, without the need of any input, allowing the AO [24], BF [25], and WR [26] models to be treated. Here we combine these tools to derive a DFT for ternary systems.

In Sec. II we define the model ternary mixtures of spheres, polymers, and needles. In Sec. III the DFT is developed. Application to bulk phases in Sec. IV yields the phase behavior. We finish with concluding remarks in Sec. V.

II. THE MODEL

We consider a mixture of colloidal hard spheres (species C) of radius R_C, globular polymers (species P) of radius R_P, and vanishingly thin needles (species N) of length L, with respective number densities $\rho_C(\mathbf{r})$, $\rho_P(\mathbf{r})$, and $\rho_N(\mathbf{r},\mathbf{\Omega})$, where $\mathbf{r}$ is the spatial coordinate and $\mathbf{\Omega}$ is a unit vector pointing along the needle axis (see Fig. 1). The pair interaction between colloids is $V_{CC}=\infty$ if the separation r between sphere centers is less than $2R_C$, and zero otherwise. The pair interactions between like particles of both other components vanish for all distances: $V_{PP}=V_{NN}=0$. For polymers this is an assumption strictly valid only at the theta point; for needles it becomes exact in the present limit of large aspect ratio, where overlapping needles contribute a

*Permanent address: Institut für Theoretische Physik II, Heinrich-Heine-Universität Düsseldorf, Universitätsstraße 1, D-40225 Düsseldorf, Germany.
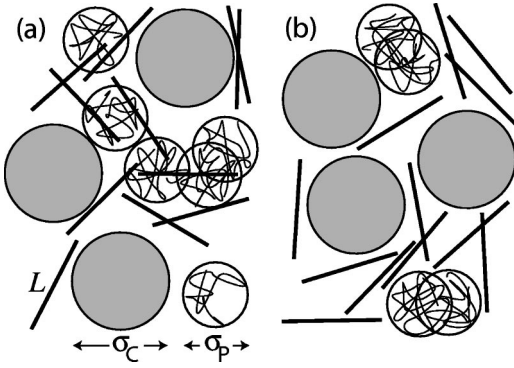
FIG. 1. Sketch of the ternary mixture of colloidal hard spheres with diameter σ_C, ideal polymer spheres of diameter σ_P and vanishingly thin needles of length L. Different cases for interactions between polymers and needles are depicted: (a) no interactions; (b) excluded volume interactions.

negligible fraction of configurations. The colloidal spheres interact with both other components via excluded volume: The pair interaction between colloids and polymers is $V_{CP} = \infty$ if $r < R_C + R_P$, and zero otherwise; the interaction between colloids and needles is $V_{CN} = \infty$, if both overlap, and zero otherwise. What remains to be prescribed is the interaction between needles and polymers. We consider two cases: (i) ideal interactions such that $V_{PN} = 0$ for all distances, and (ii) excluded volume interactions such that $V_{PN} = \infty$ if needle and polymer overlap, and zero otherwise. We denote the sphere diameters by $\sigma_C = 2R_C$, $\sigma_P = 2R_P$, the sphere packing fractions by $\eta_C = 4\pi R_C^3 \rho_C/3$, $\eta_P = 4\pi R_P^3 \rho_P/3$, and use a dimensionless needle density $\rho_N^* = \rho_N L^3$.

III. DENSITY FUNCTIONAL THEORY

A. Weight functions

We start with a geometrical representation of the particles in terms of weight functions w_μ^i, where $\mu = 3, 2, 1, 0$ corresponds to the particles' volume, surface, integral mean curvature, and Euler characteristic, respectively [27], and $i = C, P, N$ labels the species. We will use S as a unifying symbol for the spherical species C and P, and denote the radius as R, where $R = R_C, R_P$ for $S = C, P$, respectively. The weight functions are determined to give the hard core Mayer bonds $f_{ij} = \exp(V_{ij}) - 1$ by a linear combination of terms $w_\gamma^i(\mathbf{r}) * w_{3-\gamma}^j(\mathbf{r})$, where the asterisk denotes the convolution, $g(\mathbf{r}) * h(\mathbf{r}) = \int d^3x\, g(\mathbf{x}) h(\mathbf{r} - \mathbf{x})$.

For spheres, the usual weight functions [23,28] are

$$w_3^S(\mathbf{r}) = \theta(R - r), \quad w_2^S(\mathbf{r}) = \delta(R - r), \quad (1)$$

$$\mathbf{w}_{v2}^S(\mathbf{r}) = w_2^S(\mathbf{r})\mathbf{r}/\tau, \quad \hat{\mathbf{w}}_{m2}^S(\mathbf{r}) = w_2^S(\mathbf{r})[\mathbf{rr}/r^2 - \hat{\mathbf{1}}/3], \quad (2)$$

where $r = |\mathbf{r}|$, $\delta(r)$ is the Dirac distribution, $\theta(r)$ is the step function, and $\hat{\mathbf{1}}$ is the identity matrix. Further linearly dependent weights are $w_1^S(\mathbf{r}) = w_2^S(\mathbf{r})/(4\pi R)$, $\mathbf{w}_{v1}^S(\mathbf{r}) = \mathbf{w}_{v2}^S(\mathbf{r})/(4\pi R)$, $w_0^S(\mathbf{r}) = w_1^S(\mathbf{r})/R$. Note that these weights have different tensorial rank: w_0^S, w_1^S, w_2^S, w_3^S are scalars;

$\mathbf{w}_{v1}^S$, $\mathbf{w}_{v2}^S$ are vectors; $\hat{\mathbf{w}}_{m2}^S$ is a (traceless) matrix. These functions give the Mayer bond between pairs of spheres [23] through $-f_{SS}/2 = w_3^S * w_0^S + w_2^S * w_1^S - \mathbf{w}_{v2}^S * \mathbf{w}_{v1}^S$. However, they are not sufficient to recover the sphere-needle Mayer bond [27]. This is achieved through

$$w_2^{SN}(\mathbf{r}, \mathbf{\Omega}) = 2|\mathbf{w}_{v2}^S(\mathbf{r}) \cdot \mathbf{\Omega}|, \quad (3)$$

which contains information about *both* species: it is nonvanishing on the surface of a sphere with radius R, but this surface is "decorated" with an $\hat{\mathbf{\Omega}}$ dependence. Furthermore, for needles, we follow Ref. [27] to obtain

$$w_1^N(\mathbf{r}, \mathbf{\Omega}) = \frac{1}{4} \int_{-L/2}^{L/2} dl\, \delta(\mathbf{r} + \hat{\mathbf{\Omega}}l), \quad (4)$$

$$w_0^N(\mathbf{r}, \mathbf{\Omega}) = \frac{1}{2}[\delta(\mathbf{r} + \hat{\mathbf{\Omega}}L/2) + \delta(\mathbf{r} - \hat{\mathbf{\Omega}}L/2)], \quad (5)$$

and $\mathbf{r}$ is the needle center of mass. The function w_1^N describes the linear extent of a needle, whereas w_0^N is characteristic of its endpoints. For vanishingly thin needles, both surface and volume vanish, and so do the corresponding weights, $w_2^N = w_3^N = 0$. Technically, the Mayer bond is generated through $-f_{SN}(\mathbf{r}, \mathbf{\Omega}) = w_3^N(\mathbf{r}) * w_0^N(\mathbf{r}, \mathbf{\Omega}) + w_2^{SN}(\mathbf{r}, \mathbf{\Omega}) * w_1^N(\mathbf{r}, \mathbf{\Omega})$, where $\mathbf{r}$ is the difference vector between sphere and needle position.

B. Weighted densities

The weight functions are used to smooth the possibly highly inhomogeneous density profiles by convolutions,

$$n_\nu^C(\mathbf{r}) = \rho_C(\mathbf{r}) * w_\nu^C(\mathbf{r}), \quad (6)$$

$$n_\nu^P(\mathbf{r}) = \rho_P(\mathbf{r}) * w_\nu^P(\mathbf{r}), \quad (7)$$

$$n_2^{CN}(\mathbf{r}, \mathbf{\Omega}) = \rho_C(\mathbf{r}) * w_2^{CN}(\mathbf{r}, \mathbf{\Omega}), \quad (8)$$

$$n_2^{PN}(\mathbf{r}, \mathbf{\Omega}) = \rho_P(\mathbf{r}) * w_2^{PN}(\mathbf{r}, \mathbf{\Omega}), \quad (9)$$

$$n_\tau^N(\mathbf{r}, \mathbf{\Omega}) = \rho_N(\mathbf{r}, \mathbf{\Omega}) * w_\tau^N(\mathbf{r}, \mathbf{\Omega}), \quad (10)$$

where $\nu = 0, 1, 2, 3, v1, v2, m2$, and $\tau = 0, 1$; $\rho_C(\mathbf{r})$, $\rho_P(\mathbf{r})$, and $\rho_N(\mathbf{r}, \mathbf{\Omega})$ are the one-body density distributions of spheres, polymers, and needles, respectively. Note that n_ν^C, n_ν^P, n_ν^N are "pure" weighted densities, involving only variables of either species [23,27]. In contrast, n_2^{CN} and n_2^{PN} are a convolution of the sphere densities with orientation-dependent weight function, combining characteristics of both species [25].

C. Free energy density

The Helmholtz excess free energy is obtained by integrating over a free energy density,

$$F_{\text{exc}}[\rho_C, \rho_P, \rho_N] = k_B T \int d^3x \int \frac{d^2\Omega}{4\pi} \Phi(\{n_\gamma^i\}), \quad (11)$$

where k_B is Boltzmann's constant, T is temperature, and the (local) reduced excess free energy density Φ is a simple function (not a functional) of the weighted densities n_γ^i. This leads to a dependence of Φ on orientation and position. The variable $\mathbf{x}$ runs over space [23,27], and $\boldsymbol{\Omega}$ over the unit sphere [25].

The functional form of Φ is obtained by consideration of the exact zero-dimensional excess free energy. We obtain

$$\Phi = \Phi_{CC} + \Phi_{CP} + \Phi_{CN} + \lambda \Phi_{PN}, \tag{12}$$

where in the case of ideal polymer-needle interaction $\lambda = 0$, and for hard polymer-needle interaction $\lambda = 1$. In the following, the arguments of the weighted densities are suppressed in the notation; see Eqs. (6)–(10) for the explicit dependence on $\mathbf{r}$ and $\boldsymbol{\Omega}$. The hard sphere contribution, being equal to the pure HS case [23,28], is

$$\Phi_{CC} = -n_0^C \ln(1 - n_3^C) + (n_1^C n_2^C - \mathbf{n}_{v1}^C \cdot \mathbf{n}_{v2}^C)/(1 - n_3^C)$$
$$+ [(n_2^C)^3/3 - n_2^C (\mathbf{n}_{v2}^C)^2 + 3(\mathbf{n}_{v2}^C \cdot \hat{\mathbf{n}}_{m2}^C \cdot \mathbf{n}_{v2}^C$$
$$- 3 \det \hat{\mathbf{n}}_{m2}^C)/2]/[8\pi(1 - n_3^C)^2]. \tag{13}$$

The contribution due to interactions between colloids and polymers is the same as in the pure AO case [24] and is given by

$$\Phi_{CP} = \sum_\nu \frac{\partial \Phi_{CC}}{\partial n_\nu^C} n_\nu^P. \tag{14}$$

The contribution due to interactions between colloids and needles [25] is

$$\Phi_{CN} = -n_0^N \ln(1 - n_3^C) + \frac{n_1^N n_2^{CN}}{1 - n_3^C}. \tag{15}$$

Note that the simultaneous presence of Φ_{CP} and Φ_{CN} in Φ does not generate artificial interactions between P and N. For vanishing PN pair potential one can derive these terms from consideration of multicavity distributions like in the binary CP [24,12] and CN cases [25]. In order to model the WR-type interaction between polymers and needles in the presence of the colloidal spheres we use

$$\Phi_{PN} = \frac{n_0^N n_3^P + n_1^N n_2^{PN}}{1 - n_3^C}. \tag{16}$$

This can be derived as follows. The starting point is a functional for binary hard spheres with added needles. Linearization in one of the sphere densities (which becomes the polymer species) is performed in the same way as linearization of binary hard spheres leads to the CP functional [12]. In the absence of colloids, we obtain $\Phi = \Phi_{PN} = n_0^N n_3^P + n_1^N n_2^{PN}$. Then the density functional can be rewritten as $F_{\mathrm{exc}} = -\int d^3r \int d^3r' \int d^2\Omega \rho_P(\mathbf{r}) f_{PN}(\mathbf{r}; \mathbf{r}', \boldsymbol{\Omega}) \rho_N(\mathbf{r}, \boldsymbol{\Omega})/(4\pi)$. This is precisely (a generalization to needles of) the mean-field DFT for the WR model [15]. Although this does

not feature the exact zero-dimensional (0d) limit, as the geometry-based DFT [26] for WR *spheres* does, we expect differences to be small.

IV. RESULTS

A. Bulk fluid phases

For homogeneous density profiles, $\rho_i = \mathrm{const}$, the integrations in Eqs. (6)–(10) can be carried out explicitly. The hard sphere contribution is equal to the Percus-Yevick compressibility (and scaled-particle) result, which is

$$\Phi_{CC} = \frac{3\eta_C[3\eta_C(2 - \eta_C) - 2(1 - \eta_C)^2 \ln(1 - \eta_C)]}{8\pi R_C^3(1 - \eta_C)^2}. \tag{17}$$

The colloid-polymer contribution is equal to that predicted by free volume theory [8], and rederived by DFT [24] as

$$\Phi_{CP} = \frac{\eta_P/(8\pi R_P^3)}{(1 - \eta_C)^3}\{3q\eta_C[6(1 - \eta_C)^2 + 3q(2 - \eta_C - \eta_C^2)$$
$$+ 2q^2(1 + \eta_C + \eta_C^2)] - 6(1 - \eta_C)^3 \ln(1 - \eta_C)\}, \tag{18}$$

where $q = \sigma_P/\sigma_C$. The colloid-needle contribution equals the perturbative (around a pure hard sphere fluid) treatment of Ref. [5], which can be shown to equal the result from application of scaled-particle theory [29], and DFT [25], and is given by

$$\Phi_{CN} = \rho_N\left[-\ln(1 - \eta_C) + \frac{3L}{4R_C}\frac{\eta_C}{1 - \eta_C}\right]. \tag{19}$$

The WR-type polymer-needle contribution is

$$\Phi_{PN} = \left(1 + \frac{3L}{4R_P}\right)\frac{\rho_N \eta_P}{1 - \eta_C}. \tag{20}$$

For completeness, the ideal free energy contribution is

$$\phi_{\mathrm{id}} = \sum_{i = C, P, N} \rho_i[\ln(\rho_i \Lambda_i^3) - 1], \tag{21}$$

where the Λ_i are (irrelevant) thermal wavelengths of species i. This puts us into a position to obtain the reduced total free energy per volume $\Phi_{\mathrm{tot}} = \Phi_{\mathrm{id}} + \Phi$ of any given fluid state characterized by the bulk densities and relative sizes of the three components.

B. Phase diagram

The general conditions for phase coexistence are equality of the total pressures p_{tot}, and of the chemical potentials μ_i in the coexisting phases. Equality of temperature is trivial in hard-body systems. For phase equilibrium between phases I and II,

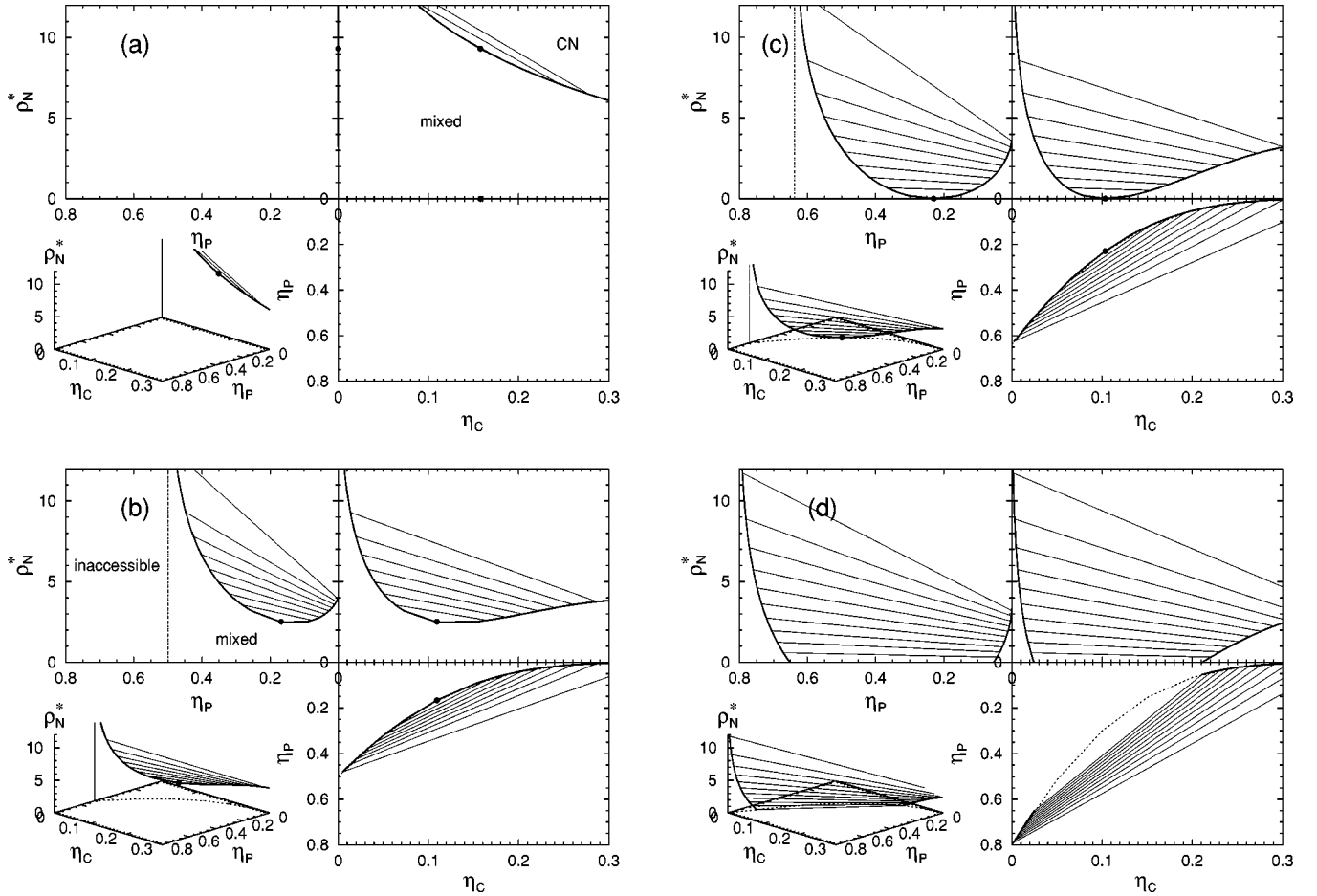$$p_{\mathrm{tot}}^{\mathrm{I}} = p_{\mathrm{tot}}^{\mathrm{II}}, \tag{22}$$

FIG. 2. Demixing phase diagram of a ternary colloid-polymer-needle mixture with ideal polymer-needle interactions for $\sigma_C = \sigma_P = L$, and $\eta_P^r = 0$ (a), 0.5 (b), 0.638 31 (c), 0.8 (d). Shown are binodals (lines), tielines between coexisting phases (thin lines), and critical points (dots).

$$\mu_i^I = \mu_i^{II}, \quad i = C, P, N. \tag{23}$$

These are four equations for six unknowns (two statepoints each characterized by three densities). Hence two-phase coexistence regions depend parametrically on two free parameters. For three-phase equilibrium between phases I, II, and III,

$$p_{tot}^I = p_{tot}^{II} = p_{tot}^{III}, \tag{24}$$

$$\mu_i^I = \mu_i^{II} = \mu_i^{III}, \quad i = C, P, N. \tag{25}$$

Eight equations for nine variables leave one free parameter.

In our case $p_{tot}/k_B T = -\Phi_{tot} + \Sigma_{i=C,P,N} \rho_i \partial \Phi_{tot}/\partial \rho_i$, and $\mu_i = k_B T \partial \Phi_{tot}/\partial \rho_i$ yield analytical expressions. We solve the resulting sets of equations numerically, which is straightforward.

1. Ideal polymer-needle interaction

Let us first explain our representation of the ternary phase diagrams. We take the system densities η_C, η_P, ρ_N^* as basic variables. For given particle sizes, these span a three-dimensional (3D) phase space. Each point in this space corresponds to a possible bulk state, at some pressure p_{tot}. Two-phase coexistence is indicated by a pair of points that are

joined by a straight tie line. Accordingly, three-phase coexistence is a triplet of points, defining a triangle. In order to graphically represent the phase diagram, we show surfaces defined by one thermodynamic parameter being constant. Such surfaces are conveniently taken such that coexistence lines (and triangles) lie completely within the surface. Clearly, this can be accommodated by imposing a constant value of p_{tot} or any of μ_C, μ_P, and μ_N. Here we choose $\mu_P = $ const, and hence imagine controlling the system directly with η_C and ρ_N^*, but indirectly via coupling to a polymer reservoir of packing fraction $\eta_P^r = (4\pi/3)(R_P/\Lambda_P)^3 \exp(\mu_P/k_B T)$. A constant-$\eta_P^r$ surface is nontrivially embedded in the 3D phase diagram. To depict it graphically, we show projections onto the three sides of the coordinate system, namely, the $\eta_C - \rho_N^*$, $\eta_C - \eta_P$, and $\eta_P - \rho_N^*$ planes, as well as a perspective 3D view. Furthermore, we indicate the accessible regions that are compatible with the constraint of fixed η_P^r. Their boundaries are implicitly defined through $\eta_P^r(\eta_C=0, \eta_P, \rho_N^*) = $ const and $\eta_P^r(\eta_C, \eta_P, \rho_N^*=0) = $ const. Note that tielines are allowed to cross inaccessible regions.

For simplicity, and to establish a reference case, we initially ignore polymer-needle interactions and consider equal particle sizes, $\sigma_C = \sigma_P = L$. In the absence of polymer (η_P^r
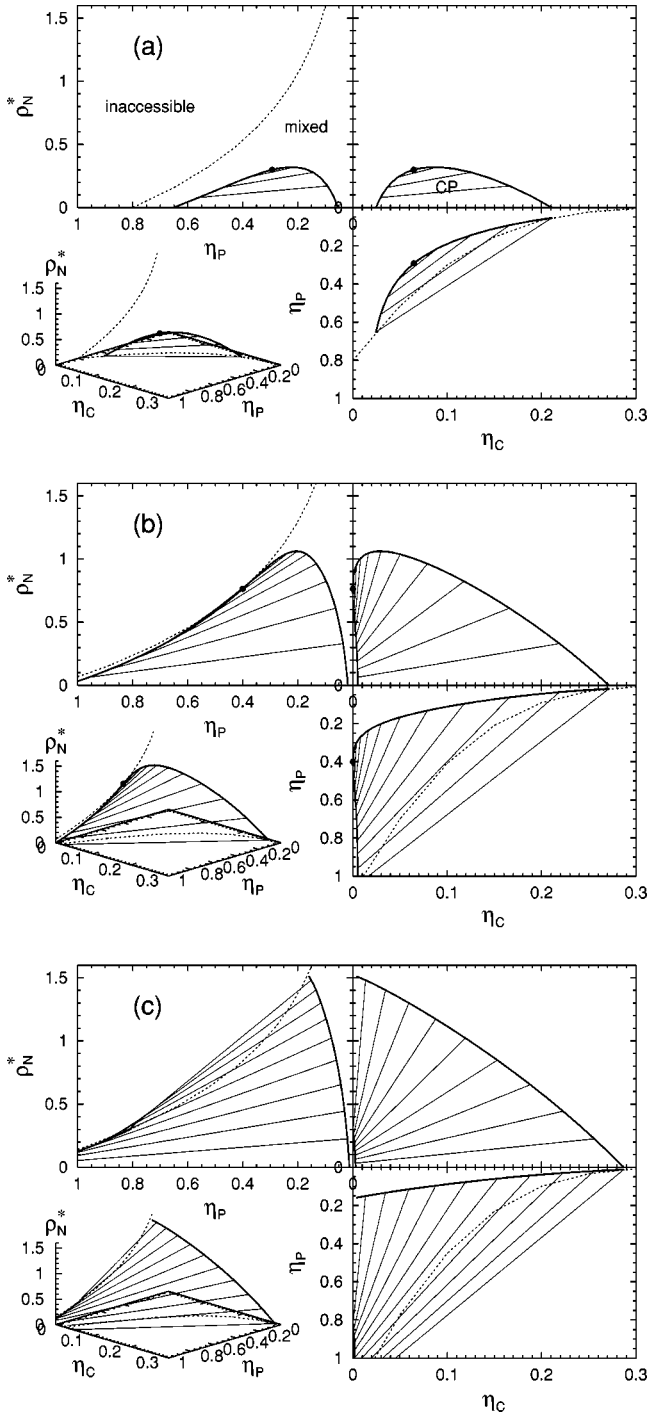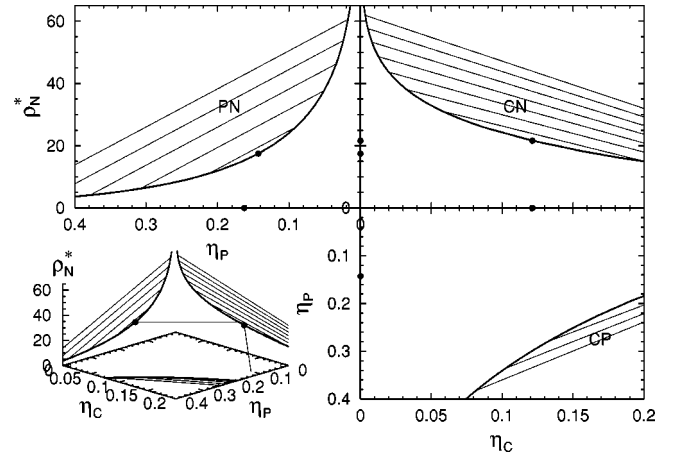
FIG. 4. Demixing phase diagrams in the binary subsystems with hard polymer-needle interactions for $\sigma_C = 2\sigma_P = L/2$.

binary CP (AO) model, which is located at $\eta_P^r = 0.638\,31$ [see Fig. 2(c)]. Computer simulations are currently being carried out to test the accuracy of this value [30]. For still larger η_P^r, the mixed states become disconnected, hence there is no path between colloid-rich and colloid-poor phases that does not pass through a first-order phase transition [see Fig. 2(d) for $\eta_P^r = 0.8$].

2. Hard polymer-needle interaction

Turning on the excluded-volume interaction between polymers and needles allows the possibility of demixing between these components. In the absence of colloids, the PN mixture is of WR type: Interactions between particles of like species vanish, while unlike particles interact with a hard core repulsion. Our case is a generalization to nonspherical particle shapes. In the mean-field treatment this does not affect the phase diagram, as only the net excluded volume enters into the theory. This robustness is also present in our approach.

We first consider equal particle sizes, $\sigma_C = \sigma_P = L$. It turns out that interesting behavior is observed only for small $\rho_N^* < 0.2$. The colloid-needle demixing curve lies well above this region, and is only weakly affected by $\eta_P^r > 0$. In the absence of needles ($\rho_N^* = 0$) and for large enough polymer density, colloids and polymers demix, indicated by a miscibility gap along the $\rho_N^* = 0$ axis [see Fig. 3(a) for $\eta_P^r = 0.8$]. Increasing needle density $\rho_N^* > 0$ causes the gap to shrink and eventually to disappear in a critical point. Quite surprisingly, and in contrast to the former case of absent *PN* interactions, the addition of needles *favors* mixing. This behavior may reflect a competition between the depleting effects of interacting polymers and needles. By analogy with the *CP* subsystem it is clear that at sufficiently high polymer density, a *PN* miscibility gap will open for $\eta_C = 0$. However, this happens not by growing a small bump as in the *CP* case. Instead the *CP* demixing curve bends over to smaller η_C and touches (with its critical point) the $\eta_C = 0$ axis (see Fig. 3(b) for $\eta_P^r = 1.087\,31$). For larger η_P^r, the critical point disappears [see Fig. 3(c) for $\eta_P^r = 1.2$].

FIG. 3. Demixing phase diagram of a ternary colloid-polymer-needle mixture with hard polymer-needle interactions for $\sigma_C = \sigma_P = L$, and $\eta_P^r = 0.8$ (a), $1.087\,31$ (b), 1.2 (c).

$= 0$), colloids and needles demix, as shown in Fig. 2(a). Increasing the packing fraction of polymers in the reservoir causes the demixed region to grow and to shift to smaller η_C and ρ_N^* [see Fig. 2(b) for $\eta_P = 0.5$]. This behavior can be understood if addition of a second depleting species simply enhances the depletion-induced attraction between colloids. Increasing η_P^r further causes the critical point to hit the $\rho_N^* = 0$ axis. This is precisely the demixing critical point of the
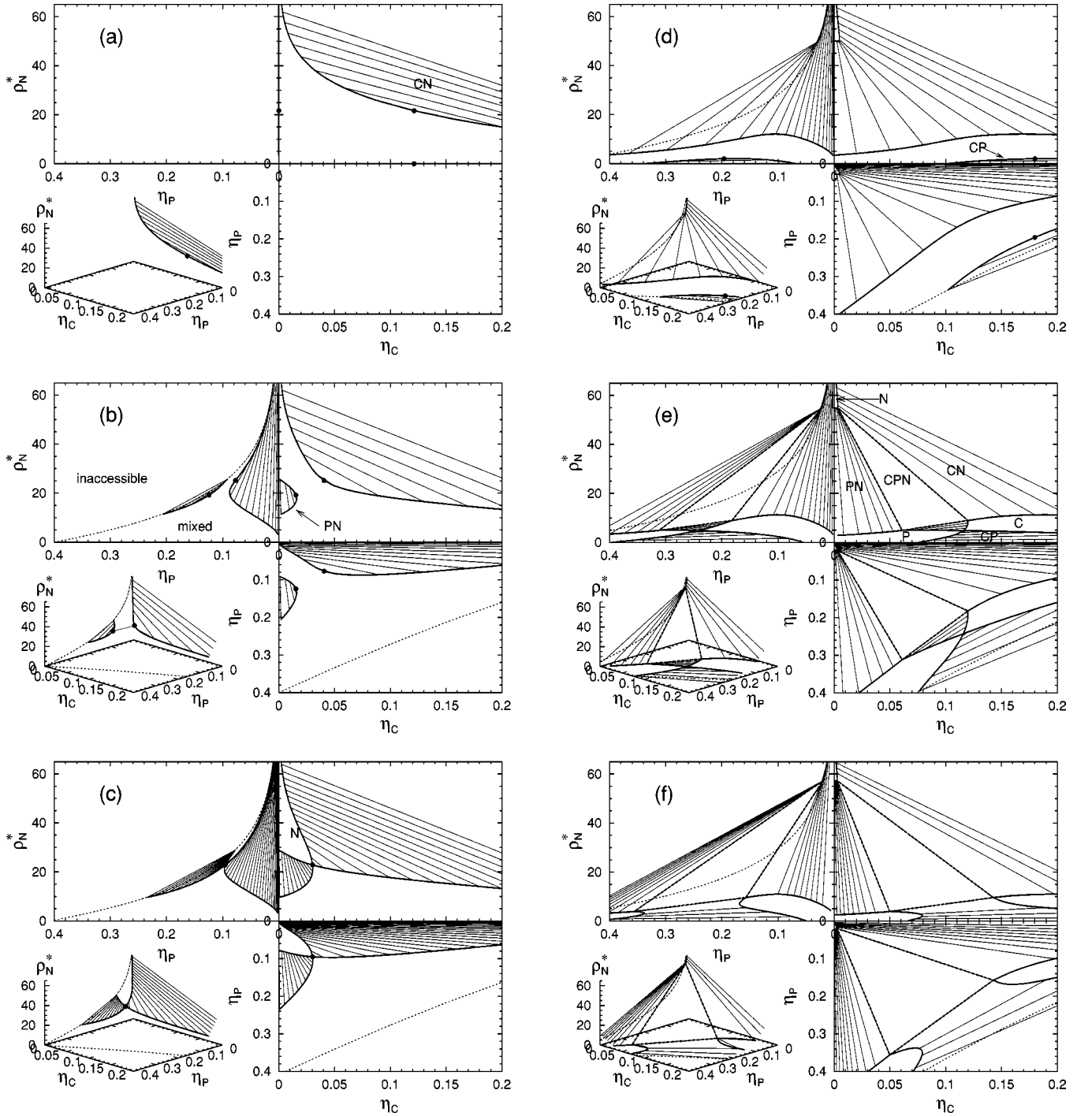
FIG. 5. Same as Fig. 3, but for $\sigma_C = 2\sigma_P = L/2$, and $\eta_P^r = 0$ (a), 0.4 (b), 0.408 107 (c), 0.5 (d), 0.526 26 (e), 0.54 (f).

In order to bring CP and CN demixing closer together, we consider a reduced polymer size $\sigma_P = \sigma_C/2$, generating a weaker depletion attraction between colloids (at the same number density of polymers), and longer needles, $L = 2\sigma_C$ generating stronger depletion between colloids, and hence lower ρ_N^* at the critical point in the binary CN case. Figure 4 shows the binodals in the (three) binary subsystems. For the ternary mixture, we follow a path of increasing η_P^r, starting with $\eta_P^r = 0$, for which the phase diagram is displayed in Fig. 5(a). There is no polymer present in the system, and phase

separation into colloid-rich and needle-rich phases occurs at high enough densities of these components. Both η_P-ρ_N^* and η_C-η_P planes are inaccessible as $\eta_P = 0$. Increasing polymer density [$\eta_P^r = 0.4$ in Fig. 5(b)] shifts the CN critical point to lower η_C, distorting the formerly rounded shape of the binodal. For $\eta_C = 0$, polymers and needles demix, as η_P^r is above the critical value for the Widom-Rowlinson type demixing of these species. The presence of colloids ($\eta_C > 0$) disturbs the PN transition; the miscibility gap narrows, eventually disappearing in a critical point, with subsequent mis-

cibility. At $\eta_P^r = 0.408\,107$ [Fig. 5(c)] the CN and PN critical points merge into a single one, and a needle-rich phase (N) becomes isolated. This coexists with a phase that consists (primarily) of colloids and polymers at varying composition. For growing η_P^r, the "double" critical point broadens into a line and results in a thin neck joining both transitions.

With increasing η_P^r the coexistence region broadens further [see Fig. 5(d) for $\eta_P^r = 0.5$]. Colloids and polymers also demix. For $\rho_N^* = 0$, the system is above the critical point for the pure AO model, and hence coexistence between colloid-rich and polymer-rich phases occurs. Again, the presence of the third component, in this case N, causes the density gap to shrink and eventually disappear with a critical point. As all binary subsystems are by now demixed, it is evident that the system will ultimately display coexistence between three phases, each one enriched by one of the components, and represented by a triangle in system representation. Each corner of the triangle corresponds to one of the three coexisting phases. The Gibbs phase rule dictates that one degree of freedom remains, which is p_{tot} or, equivalently, η_P^r (note that for hard-body systems, temperature is trivially related to pressure). It is striking, however, how this triangle develops. One might expect this to occur by the joining of existing binary coexistence regions. This is not the case. The ternary region instead grows solely out of the N-rich-poor coexistence, whereby CP coexistence is only a spectator, separated by mixed states. The initial three-phase triangle is extremely elongated (being a line as a boundary case). One corner corresponds to a needle-rich phase; both others differ only slightly in densities, one phase favoring colloids, the other polymers. Moving away from this CP edge of the triangle (by reducing ρ_N^*) leads to binary coexistence between C and P. This phase separation is reminiscent of the behavior of the pure AO model. However this reentrant coexistence is triggered by the presence of the needles, and it is separated (by mixed states) from the pure AO transition (and its region of stability in the presence of needles). In Fig. 5(e) we show results for $\eta_P^r = 0.526\,26$, where the critical points of both CP transitions have already merged, and again a neck is reminis-

cent of the formerly distinct transitions. For still larger η_P^r, the three-phase triangle grows further [see Fig. 5(f) for $\eta_P^r = 0.54$]. Ultimately, at sufficient concentration the colloids must freeze, but we disregard the solid phase in the present work. We finally note that the whole scenario is covered over a relatively small density interval $\eta_P^r = 0.4 - 0.54$, and that the packing fractions of colloids and polymers are only moderate. However, needle densities can be quite high.

V. DISCUSSION

In conclusion, we have considered a simple hard-body model for a mixture of spherical colloidal particles, globular polymer coils, and needle-shaped objects, which may represent either colloidal needles, stretched polymers or polyelectrolytes. We have extended a recent DFT approach to this model and applied it to bulk fluid phases. The resulting phase behavior is very rich, ensuing from competition of demixing in the binary subsystems.

The present paper has interesting implications for the techniques of integrating out degrees of freedom (see e.g., [31,32]). Note that by integrating out, e.g., the needles, effective interactions between pairs of colloids, pairs of polymers, as well as colloids and polymers arise. Hence one arrives at a binary mixture with (soft) depletion interactions. To what extent the ultimate mapping onto a one-component (colloid) system, by further integrating out the polymers, can be achieved is an interesting question. As a further outlook, the inclusion of freezing of colloids, disregarded in the present work, would further enrich the phase behavior. Computer simulations are desirable to test the theoretical phase diagrams. Furthermore it is interesting to elucidate the structural correlations present in the various fluid phases. Inhomogeneous situations, such as induced by walls or present at interfaces between demixed states, constitute further exciting directions of research.

[1] S. Asakura and F. Oosawa, J. Chem. Phys. **22**, 1255 (1954).

[2] G. A. Vliegenthart and H. N. W. Lekkerkerker, J. Chem. Phys. **111**, 4153 (1999).

[3] S. G. J. M. Kluijtmans, G. H. Koenderink, and A. P. Philipse, Phys. Rev. E **61**, 626 (2000).

[4] A. Vrij, Pure Appl. Chem. **48**, 471 (1976).

[5] P. Bolhuis and D. Frenkel, J. Chem. Phys. **101**, 9869 (1994).

[6] B. Widom and J. S. Rowlinson, J. Chem. Phys. **52**, 1670 (1970).

[7] A. P. Gast, C. K. Hall, and W. B. Russell, J. Colloid Interface Sci. **96**, 251 (1983).

[8] H. N. W. Lekkerkerker, W. C. K. Poon, P. N. Pusey, A. Stroobants, and P. B. Warren, Europhys. Lett. **20**, 559 (1992).

[9] M. Dijkstra, J. M. Brader, and R. Evans, J. Phys.: Condens. Matter **11**, 10 079 (1999).

[10] A. A. Louis, R. Finken, and J. Hansen, Europhys. Lett. **46**, 741 (1999).

[11] M. Dijkstra, R. van Roij, and R. Evans, J. Chem. Phys. **113**, 4799 (2000).

[12] J. M. Brader, Ph.D. thesis, University of Bristol, 2001.

[13] M. I. Guerrero, J. S. Rowlinson, and G. Morrison, J. Chem. Soc., Faraday Trans. 2 **72**, 1970 (1976).

[14] J. S. Rowlinson, Adv. Chem. Phys. **41**, 1 (1980).

[15] J. S. Rowlinson and B. Widom, *Molecular Theory of Capillarity* (Clarendon, Oxford, 1982).

[16] C. Y. Shew and A. Yethiraj, J. Chem. Phys. **104**, 7665 (1996).

[17] A. Yethiraj and G. Stell, J. Stat. Phys. **100**, 39 (2000).

[18] E. Bergmann, Mol. Phys. **32**, 237 (1976).

[19] G. Johnson, H. Gould, J. Machta, and L. K. Chayes, Phys. Rev. Lett. **79**, 2612 (1997).

[20] P. Borgelt, C. Hoheisel, and G. Stell, J. Chem. Phys. **92**, 6161 (1990).

[21] *Coatings Technology Handbook*, edited by D. Satas (Dekker, New York, 1991).

[22] R. Evans, in *Fundamentals of Inhomogeneous Fluids*, edited by D. Henderson (Dekker, New York, 1992), p. 85.

[23] Y. Rosenfeld, Phys. Rev. Lett. **63**, 980 (1989).

[24] M. Schmidt, H. Löwen, J. M. Brader, and R. Evans, Phys. Rev. Lett. **85**, 1934 (2000).

[25] M. Schmidt, Phys. Rev. E **63**, R05201 (2001).

[26] M. Schmidt, Phys. Rev. E **63**, R01101 (2001).

[27] Y. Rosenfeld, Phys. Rev. E **50**, R3318 (1994).

[28] P. Tarazona, Phys. Rev. Lett. **84**, 694 (2000).

[29] J. A. Barker and D. Henderson, Rev. Mod. Phys. **48**, 587 (1976).

[30] M. Dijkstra (unpublished).

[31] J. M. Brader and R. Evans, Europhys. Lett. **49**, 678 (2000).

[32] J. M. Brader, M. Dijkstra, and R. Evans, Phys. Rev. E **63**, 041405 (2001).